Bergische Universität Wuppertal

Fakultät für Mathematik und Naturwissenschaften

Institute of Mathematical Modelling, Analysis and Computational Mathematics (IMACM)

Preprint BUW-IMACM 23/03

Sergey Pereselkov, Venedikt Kuz'kin, Matthias Ehrhardt, Sergey Tkachenko, and Pavel Rybyanets

Use of Interference Patterns to Control Sound Field Focusing in Shallow Water

January 11, 2023

http://www.imacm.uni-wuppertal.de

Article

Use of Interference Patterns to Control Sound Field Focusing in Shallow Water

Sergey Pereselkov[1,*], Venedikt Kuz'kin[2], Matthias Ehrhardt[3], Sergey Tkachenko[1] and Pavel Rybyanets[1]

[1] Voronezh State University, Russia; pereselkov@yandex.ru
[2] Prokhorov General Physics Institute of the Russian Academy of Sciences, Russia; kumiov@yandex.ru
[3] University of Wuppertal, Gaußstraße 20, 42119 Wuppertal, Germany; ehrhardt@uni-wuppertal.de
* pereselkov@yandex.ru

Abstract: The possibility of controlling localized fields in multimode shallow water waveguides based on the principle of interference invariance is studied. Within framework of the numerical experiments in a wide frequency range of 100 - 350 Hz and range intervals of 10 - 100 km, the possibilities of focusing the sound field by wavefront reversal and controlling of the focusing of the focal spot by frequency tuning in shallow water waveguide is analysed. The focal spot scanning is carried out by frequency tunning with a fixed distribution of the sound field at receiving and transmitting vertical antenna aperture. A comparative analysis of the features of focusing and focal spot control for summer and winter stratification of the water layer is carried out. It is shown that the parameters of the focal spot during frequency tuning are more stable in the winter waveguide. It is demonstrated that the sound frequency tuning has a piecewise continuous character and is carried out on a domain of one continuous track and jump-passing on other track in accordance with the waveguide interference fringes in range-frequency domain.

Keywords: shallow water; sound field; modes interference; field focusing; focusing control

1. Introduction

The problem of localization of the field at a given point of a regular ocean waveguide based on the principle of phase conjugation (*wavefront reversal* - WFR) was apparently first discussed in [1–3]. The WFR - spatial focusing consists of recording the sound field from a distant probe source by *receiving and transmitting vertical antenna* (RTA), reversing the recording signals by phase conjugation and propagating the reversed signal back in ocean waveguide. In result the sound field is spatially focused by WFR at the probe source location.

These studies of WFR in ocean waveguide were developed in [4–13]. In [4] the behavior of acoustic phase-conjugate arrays is illustrated in several examples, some highly idealized and some more realistic. The effects of apertures size and inhomogeneities in the propagation medium are treated for both the near-field and far-field regions. It is concluded that phase-conjugate arrays offer an attractive approach to some long-standing problems in underwater acoustics. In [5] the theoretical narrow-band performance of acoustic phase-conjugate arrays in the presence of static and dynamic random media is presented. For a static random medium, analytical formulas are derived for the mean focus field of a Gaussian-shaded volumetric phase-conjugate array. In [12,13] temporal and spatial focusing properties of time-reversal mirrors are studied in a waveguide. The width of the focal spot, and the spatial and temporal sidelobe levels are experimentally and numerically analyzed with respect to the characteristics of the waveguide. In [10] an experiment conducted in the Mediterranean Sea in April 1996 demonstrated that a time-reversal mirror (or phase conjugate array) can be implemented to spatially and temporally refocus an incident acoustic field back to its origin. In [11] the waveguide time-reversal mirror technique is extended to refocus at ranges other than that of the probe source. This procedure is based on the acoustic-field invariant property in the coordinates of frequency and range in an oceanic waveguide. In [7] an example of active focusing within the waveguide using the first invariant of the time reversal operator is presented, showing the enhanced focusing capability. Furthermore, the localization of the scatterers in the water

Citation: Pereselkov, S.; Kuz'kin, V.; Ehrhardt, M.; Tkachenko, S.; Rybyanets P. Use of Interference Patterns to Control Sound Field Focusing in Shallow Water. *Preprints* **2023**, *1*, 0. https://doi.org/

column is obtained using a range-dependent acoustic model. In [8] a time reversal mirror refocuses back at the original probe source position. A goal has been to refocus at different positions without model based calculations. In [9] a method is introduced for using a pair of RTAs to produce time-reversal focusing field at any location in a range-independent shallow-ocean waveguide. In [16,17] the problems of formation of acoustic fields of a certain structure in multimode waveguides are most extensively treated

The practical needs of remote sensing of inhomogeneities of the oceanic environment lead to the task of controlling the focusing (localization) of sound fields in planar multimode shallow water waveguides. The application of the traditional approach to scanning the ocean with a focal spot at range and depth, combined with the rearrangement of the field distribution at the aperture, leads to a considerable complication and an increase in the cost of a large-scale experiment. This situation forces us to investigate and test fundamentally new approaches to this problem that are realistic from an experimental point of view. The principle of interference invariance, for example, fulfills this goal [18–22]. This principle is based on the idea that the phase changes of a group of similar modes caused by variations in the observation conditions can be compensated by shifting the radiation frequency. The theory of interference invariance was constructed and confirmed by numerous experiments with respect to a point source. Its generalization to the case of an extended vertical antenna, where the same type of mode groups are excited differently at different horizons, is not obvious and deserves detailed study. In this paper, which is a further development of the ideas of [18–22], the results of numerical simulation of the control of localized wavefields by adjusting the radiation frequency without changing the distribution of the initial field along the aperture are presented.

The aim of the paper presents the results of a study of the possibility and effectiveness of focusing control based on WFR by frequency tuning without changing the distribution of the reversed field at the RTA. The focal spot scanning method is based on waveguide dispersion, which makes it possible to equalize changes in the phase modes by changing the frequency of radiation. This paper consists of five sections. The Sec.1 is introduction. In Sec.2 the general principles of focusing the sound field based on the WFR are considered. The parameters of focal spot that are used to characterize the quality of localization of the wave field are determined. The results of a comparative analysis of the localization of the sound field in summer waveguide and winter waveguide are presented. In Sec.3 the comparative analysis structure of the interferogram and hologram of sound field in the vicinity of focal spot in summer waveguide and winter waveguide are considered. In Sec.4 the possibility of scanning with a focal spot by frequency tuning the is analyzed. The nature of the radiation frequency adjustment is established. The effect of spatial repeatability of focal spots is analyzed. The Sec.5 is conclusion.

2. Sound Field Focalization Parameters in Shallow Water Waveguide

Let us consider an oceanic waveguide in a Cartesian coordinate system (r, z) as a layer of water bounded in depth by the sea surface ($z = 0$) and the flat bottom surface ($z = H$). The oceanic waveguide model and problem geometry are shown in Fig. 1. The depth-dependent refractive index and density of the water layer are $n(z)$, $\rho(z)$. The constant refractive index and density of the bottom are $n_b\,(1 + \mathrm{i}\alpha)$, ρ_b. The parameter α is determined by the absorption properties of the bottom.

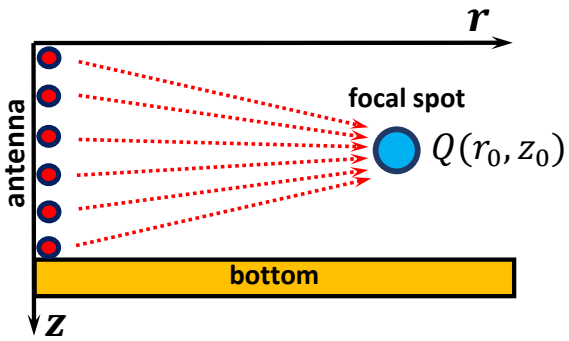

Figure 1. Sound field focalization by wavefront reversal in shallow water.

The *receiving and transmitting antenna* (RTA) is located at the coordinate origin ($r = 0$) (see Fig. 1). It consists of non-directional point receiving and transmitting elements that are equidistant at depths $z_i = (i-1)d_A$, $(i = 1, 2, \ldots, N_A)$, where d_A is the antenna period and N_A is the number of antenna elements. The upper element is located on the surface, $z_1 = 0$, and the lower element of the antenna is on the bottom $z_{N_A} = H$. It is assumed that the point monochromatic probe source is located in the *reference point* (RP) of the field focus $Q(r_0, z_0)$.

Let us describe the distribution of sources in the case of focusing the array field on the RP Q_0. We represent the vertical field distribution with frequency f_0 at the coordinate origin generated by a point source at RP Q_0 in terms of a finite sum of normal modes of a discrete spectrum:

$$w_0(0, z) = \sum_{m=1}^{M} w_m(0, z), \tag{1}$$

where

$$w_m(0, z) = \sqrt{\rho_0 c_0}\, \frac{\psi_m(r_0, z_0)\psi_m(0, z)}{\sqrt{\xi_m(0) r_0}}\, \exp\Big(\frac{\mathrm{i}\pi}{4}\Big)\, \exp\Big[\mathrm{i}\int_0^{r_0} \xi_m(r_0 - r')\, dr'\Big]. \tag{2}$$

Here, $\rho_0 = \rho(r_0, z_0)$ and $c_0 = c(r_0, z_0)$ are the water density and the sound velocity at distance r_0 and depth z_0, $\psi_m(r, z)$ and $\xi_m(r)$ are the eigenfunctions and the propagation factor of the m-th mode, and M is the number of propagating modes. In Eq. (2), the power of the source is assumed to be equal to one. The principle of phase conjugation assumes that the sound field radiated from the i-th element of the antenna array is phase conjugate to the received sound field $w_0(0, z_i)$ Eq. (1) at the i-th element point, i.e., the radiated sound field is:

$$W_i = \eta_0\, |w_0(0, z_i)|^2\, W_0. \tag{3}$$

In the absence of interactions between the array elements, the expression for the proportionality coefficient η_0 can be obtained from the normalization condition $\sum_{i=1}^{I} W_i = W_0$ given by Eq. (3) in the form:

$$\eta_0 = \Big[\sum_{i=1}^{I} |w_0(0, z_i)|^2\Big]^{-1}. \tag{4}$$

Such a phase distribution of sources produces a conjugate field, i.e., a field converging to the RP Q_0. Let us sum up the fields of the point sources. In this case, the radiation field of the array $u(r, z)$ can be reduced to the following form using the Eqs. (3), (4)

$$u(r, z) = \sum_{m=1}^{M} u_m(r, z), \tag{5}$$

where

$$u_m(r,z) = a_m \frac{\psi_m(r,z)}{\sqrt{\xi_m(r)r}} \exp\Big[\mathrm{i}\int_0^r \xi_m(r')dr'\Big], \tag{6}$$

with

$$a_m = \sqrt{\eta_0 W_0}\, \exp\Big(\frac{\mathrm{i}\pi}{4}\Big) \sum_{i=1}^{I} \sqrt{\rho_i c_i}\, w_0^*(0,z_i)\, \psi_m(0,z_i). \tag{7}$$

The focusing of the field by *wavefront reversal* (WFR) at frequency f_0 at the reference point is as follows. The field $G(r_0,0;z_0,z_i)$ generated by the PS is registered at the RTA at frequency f_0. A source distribution is generated at the RTA aperture that is phase-conjugate with the received field $KG^*(0,r_0;z_i,z_0)$. The coefficient is then assumed to be $K=1$. Such a distribution of the field at the aperture of the RTA excites an inverted wave localized at the point $Q(r_0,z_0)$:

$$\Psi(r,z,f) = \sum_{i=1}^{N_A} G(0,r;z_i,z;f)\, G^*(r_0,0;z_0,z_i;f_0). \tag{8}$$

The complex sound pressure of RP: $Q(r_0,z_0)$ in points of RTA elements: $z_i = (i-1)d_A$, $(i=1,2,\ldots,N_A)$ can be written as follows:

$$G(r_0,0;z_0,z_i;f_0) = S(f_0)\frac{\mathrm{i}\,e^{-\mathrm{i}\pi/4}}{\rho(z_0)\sqrt{8\pi}} \sum_{m=1}^{M} \frac{\phi_m(z_0,f_0)\phi_m(z_i,f_0)\exp[\mathrm{i}r_0 h_m(f_0)]}{\sqrt{r_0 h_m(f_0)}}. \tag{9}$$

Thus,

$$G(0,r;z_i,z;f) = \frac{\mathrm{i}\,e^{-\mathrm{i}\pi/4}}{\rho(z_i)\sqrt{8\pi}} \sum_{m=1}^{M} \frac{\phi_m(z_i,f)\phi_m(z,f)\exp[\mathrm{i}r h_m(f)]}{\sqrt{r h_m(f)}}. \tag{10}$$

Let us now consider the parameters of sound field focalization. The quality of localization of the field is determined by the focusing factor g, the bandwidth Δf and the geometrical dimensions of the focal peak - horizontally Δr and vertically Δz (see Fig. 2). The focusing factor characterizes the excess of the mean (background) level $\overline{|\Psi|}$ near the focal spot level at frequency f_0:

$$g(f) = \frac{|\Psi(r_0,z_0,f)|}{\overline{|\Psi|}}. \tag{11}$$

The magnitude of the focusing factor characterizes the contrast of the focal spot in relation to the sound field. The value of the average level of the sound field is determined by the neighborhood in the plane of the waveguide:

$$\overline{|\Psi|} = \frac{1}{2\Delta_r H}\int_{r_0-\Delta_r}^{r_0+\Delta_r}\int_0^H |\Psi(r,z,f_0)|\, dzdr. \tag{12}$$

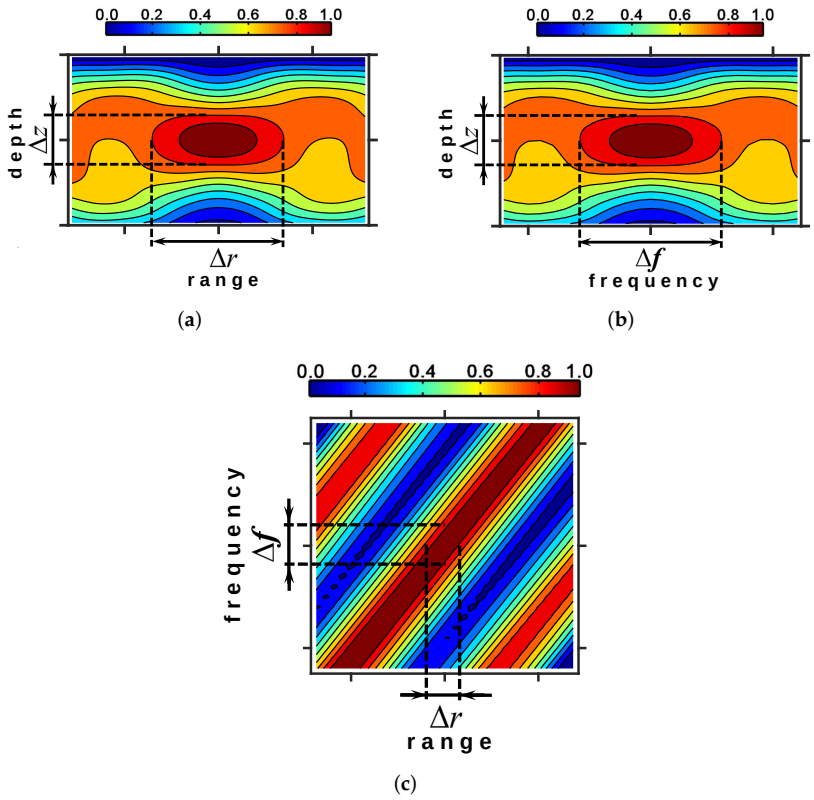

Figure 2. The sound field focal point parameters in shallow water waveguide.

The width of the band and the geometrical dimensions of the focal spot characterizing its blur are determined by a fixed level from the maximum value of the field near the localization point. Another parameter of the sound field focalization is $\delta z(r)$, the absolute value of the difference between z_0 (the depth of the reference point Q) and z_0' (the depth of the interference maximum nearest to Q):

$$\delta z = |z_0 - z_0'|. \tag{13}$$

Let us consider the characteristics of field focusing by WFR in a shallow water waveguide. We consider the influence of water layer stratification and absorption at the waveguide bottom on the quality of sound field focusing for different ranges and depths of the localization point Q and for different sound frequencies. As an example, we consider a shallow water waveguide with parameters corresponding to the experiments of JUSREX (1992) [23] and SWARM (1995) [24]. The water stratifications of these experiments are shown in Fig. 2. Fig. 2 a) corresponds to JUSREX (1992). Fig. 2 b) corresponds to SWARM (1995). Curve 1 in Fig. 2 is the water stratification in the winter season - winter waveguide (WW). Curve 2 in Fig. 2 is the water stratification in the summer season - summer waveguide (SW). Water layer depth is $H = 72$ m. Bottom parameters: $c_b = 1700$ m/s, $\rho_b = 1.8$ g/cm^3, $\alpha_b = 0.02$. RTA parameters: $d_A = 3$ m, $N_A = 25$. Sound radiation frequencies: $f_1 = 150$ Hz, $f_2 = 300$ Hz.

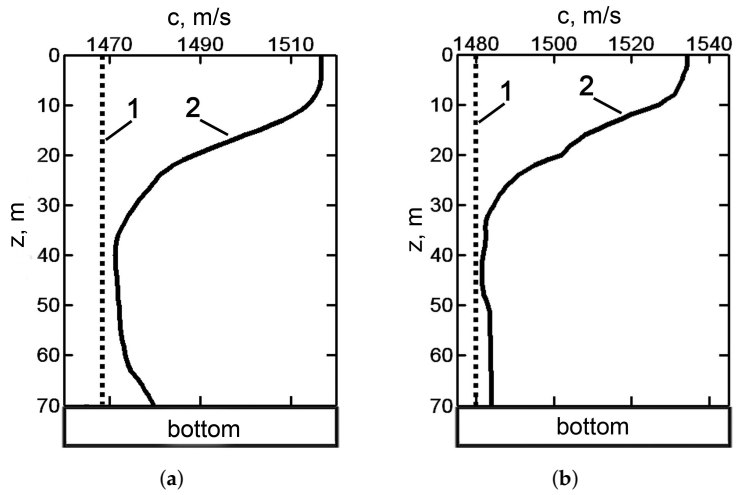

Figure 3. Sound speed profile $c(z)$. a) experiment JUSREX (1992) [23]; b) experiment SWARM'95 (1995) [24]. Curve 1 - winter waveguide (WW). Curve 2 - summer waveguide (SW).

Let us consider the following reference points: $Q_{ij}(r_i, z_j)$, where $r_1 = 10$ km, $r_2 = 50$ km, $r_3 = 100$ km; $z_1 = 10$ m, $z_2 = 35$ m, $z_3 = 60$ m. The results of numerical modeling for the reference points Q_{ij} are shown in Figs. 4 – 8. The Figs. 4 – 5 show the brightness patterns of the normalized sound field $|\Psi(r, z)|$ in the vicinity of the localization point $Q_{i_1}(r_i, z_1 = 10$ m) for WW and SW at different distances ($r_1 = 10$ km, $r_2 = 50$ km, $r_3 = 100$ km) from the RTA. Fig. 4 corresponds to $f_1 = 150$ Hz, Fig. 5 $f_2 = 300$ Hz.

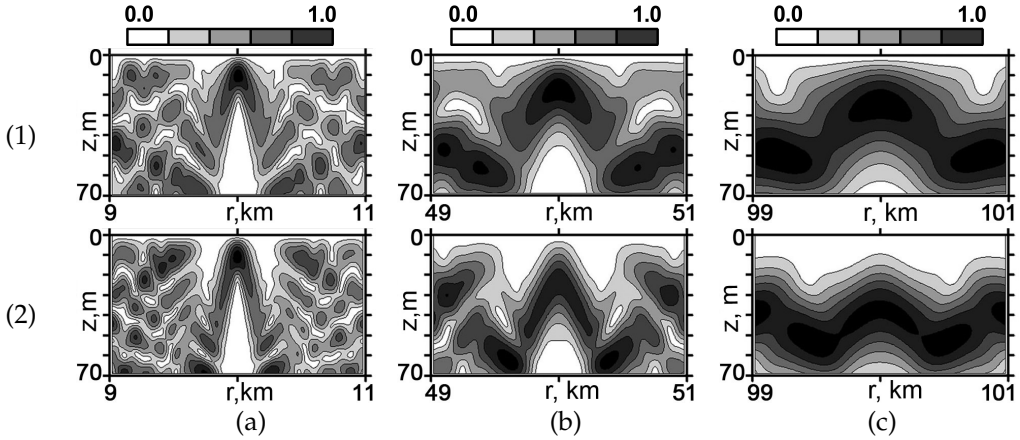

Figure 4. Normalized sound field distribution near focal point $|\Psi(r, z)|$ at a frequency of $f_1 = 150$ Hz. 1) SWARM'95 (WW). 2) SWARM'95 (SW). a) $Q(r_1 = 10$ km, $z_1 = 10$m); b) $Q(r_2 = 50$ km, $z_2 = 10$ m); c) $Q(r_3 = 100$ km, $z_3 = 10$ m).

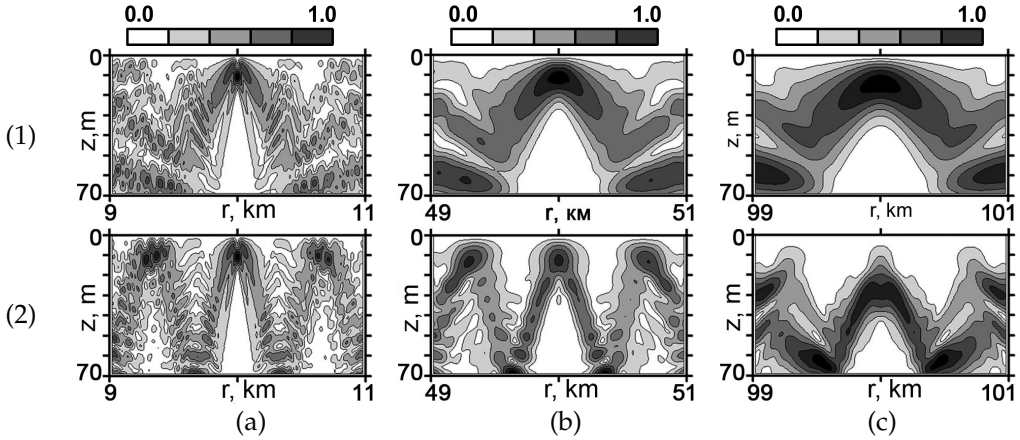

Figure 5. Normalized sound field distribution near focal point $|\Psi(r,z)|$ at a frequency of $f_1 = 300$ Hz. 1) SWARM'95 (WW). 2) SWARM'95 (SW). a) $Q(r_1 = 10$ km, $z_1 = 10$ m); b) $Q(r_2 = 50$ km, $z_2 = 10$ m); c) $Q(r_3 = 100$ km, $z_3 = 10$ m).

As can be seen from Figs. 4 – 5, as the distance from the localization point of the field $Q(r_0, z_0)$ increases, the longitudinal and transverse dimensions of the focal spot increase. For example, for SW at a distance of $r_1 = 10$ km at a frequency of $f_1 = 150$ Hz, the dimensions of the focal spot are $\Delta z = 7.7$ m, $\Delta r = 80$ m. For a frequency of $f_2 = 300$ Hz - $\Delta z = 3.9$ m, $\Delta r = 30$ m. For a distance of $r_3 = 100$ km and a frequency of $f_1 = 150$ Hz, the dimensions of the focal spot are $\Delta z = 16.4$ m, $\Delta r = 224$ m. For a frequency of $f_2 = 300$ Hz - $\Delta z = 9.6$ m, $\Delta r = 126$ m.

A similar behavior of the focal spot parameters is also observed for WW. This effect is explained by the manifestation of bottom absorption, by which with increasing distance the fraction of modes with high numbers, responsible for the small-scale structure of the field, decreases. As a result, the spatial distribution of the field in the localization region becomes smoother with increasing distance. This in turn leads to a decrease in the contrast of the focal spot, i.e., a decrease in the focus factor. For a SW at a distance of $r_1 = 10$ km at a frequency of $f_1 = 150$ Hz -$g = 5.11$, at a frequency of $f_2 = 300$ Hz - $g = 8.73$. At a distance of $r_3 = 100$ km at a frequency of $f_1 = 150$ Hz - $g = 2.47$, at a frequency of $f_2 = 300$ Hz -$g = 4.14$.

Fig. 6 shows the dependence of the focusing factor $g(r)$ (a) and the horizontal size $\Delta r(r)$ of the focal spot (b) on the distance to the localization point. The results are related to the SW. Note that such a characteristic decrease of the focusing factor and an increase of the transverse dimension $\Delta r(r)$ is practically independent of the depth of the focusing point and the channel stratification.

Fig. 7 shows the dependence of the longitudinal size $\Delta z(r)$ of the focal spot on the distance to the localization point. Fig. 7 a) corresponds to WW, Fig. 7 b) - SW. As can be seen, faster growth is observed in WW than in SW. This is explained by the less uniform depth distribution of the modes in the waveguide with summer stratification.

In a shallow water waveguide, with the increase of the geometrical dimensions of the focal spot Δr, Δz and with the decrease of the focusing factor g, another effect is observed. It consists in the displacement of the focal spot from the position of the localization point in depth. To illustrate this effect, Fig. 8 shows the dependence $\delta z(r)$ on the absolute value of the difference between z_0 (the depth of RP Q) and z_0' (the depth of the interference maximum closest to Q). As can be seen, the focal spot is most displaced from the RP position near the free surface of the sound channel at frequencies of $f_1 = 150$ Hz and $f_2 = 300$ Hz: $Q_{01}(r_0, z_0 = 10$ m).

Moreover, in the sound channel with summer stratification, this effect is most pronounced. At a distance of 100 km for a frequency of $f_1 = 150$ Hz, the shift of the focal spot from $Q(r_0, z_0 = 10$ m) in the SW is $\Delta z = 27$ m. This is approximately twice as much

as compared to the WW, in which $\Delta z = 14$ m. At the same time, at a high frequency $f_2 = 300$Hz, the displacement does not exceed two meters in the WW for all considered depths. This situation persists over the entire considered range of distances from 10 km to 100 km. A similar situation is also observed in the SW for localization points under the thermocline, but for $Q(r_0, z_0 = 10$ m) it sharply increases to the value of $\Delta z = 17$ m at a distance of 100 km.

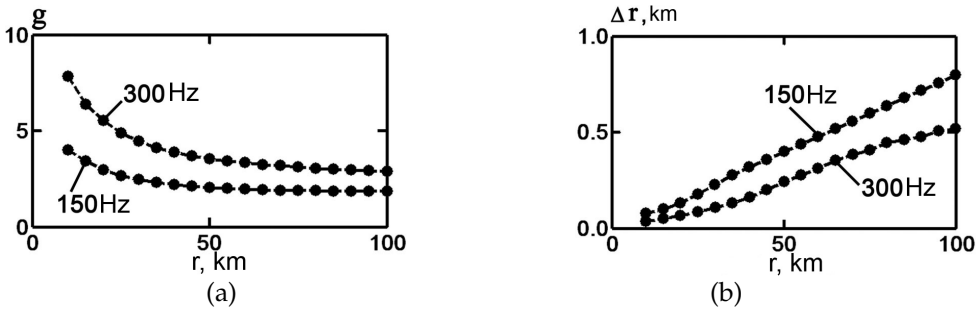

Figure 6. Distance dependence of focusing factor g (a), longitudinal size Δr (b) of the focal spot. SW, $Q(r, z = 35$ m).

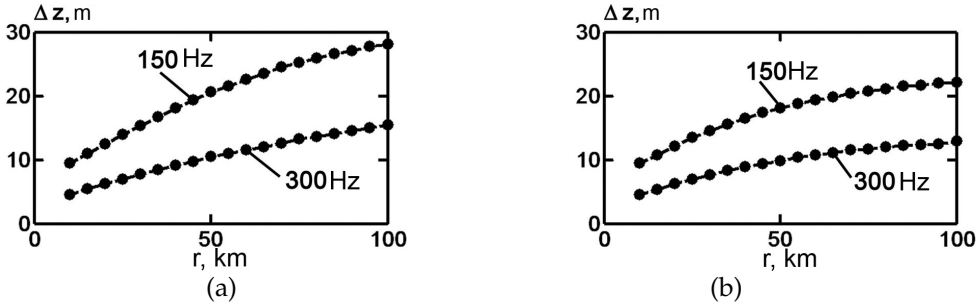

Figure 7. Dependence of the transverse size of the focal spot Δz on the distance for the observation point $Q(r, z = 35$ m) : a) WW; b) SW.

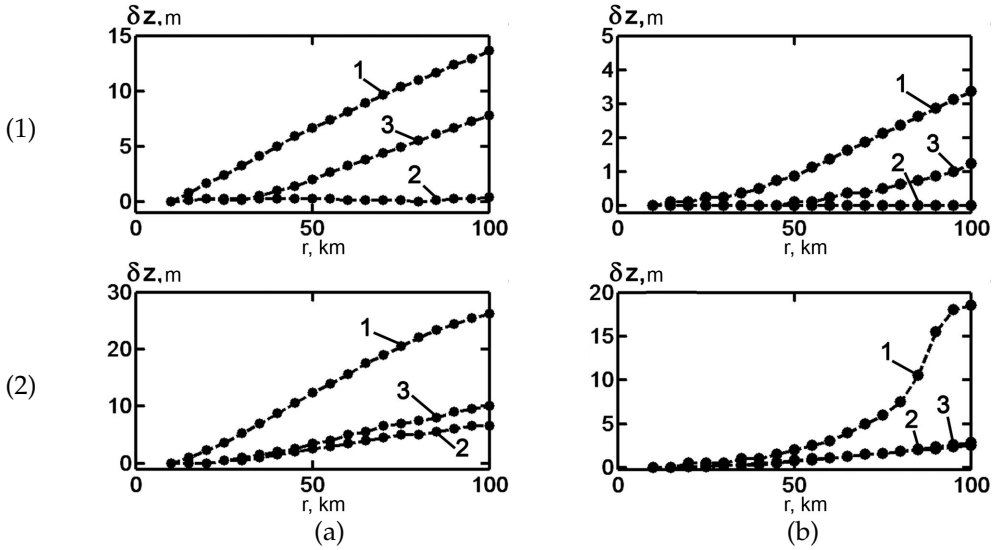

Figure 8. The dependence of the displacement of δz focal spot on the distance: a) $f_1 = 150$ Hz, b) $f_2 = 300$ Hz. 1) WW; 2) SW. Curve 1 - $Q(r, z = 10$ m); Curve 2 - $Q(r, z = 35$ m); Curve 3 – $Q(r, z = 60$ m).

3. Interferogram and Hologram of the Sound Field in the Focalization Point

The intensity of a field of frequency ω at a horizontal distance r from the source can be represented as the sum of propagating interacting modes:

$$I(r,\omega) = \sum_m \sum_n C_m(r)\, C_n^*(r)\, \exp\left[\mathrm{i}\int_0^r q_{mn}(\omega, r')\, dr'\right], \tag{14}$$

where C_m is the mode amplitude and q_m the horizontal wavenumber of the $m-th$ mode. Here $q_{mn} = q_m - q_n$. In the vicinity of the point (ω_0, r_0) some local intensity extremum ϑ_0 maximum level lines $I(r,\omega)$ in the coordinate system of relative increments of distance and frequency has the following form [19]:

$$\beta = \frac{\Delta\omega/\omega_0}{\Delta r/r_0} = (r_0/\omega_0)\mathrm{tg}\,\vartheta_0 = -\frac{r_0}{\omega_0}\frac{\partial I(r_0,\omega_0)/\partial r}{\partial I(r_0,\omega_0)/\partial\omega}. \tag{15}$$

Here, $\Delta\omega = \omega - \omega_0$, $\Delta r = r - r_0$ are frequency and distance increments corresponding to the shift of the considered field extremum on the distance-frequency plane. The value β is called waveguide *interference invariant* (II) of the sound field.

3.1. Differential Approach

Most work examining various aspects of β uses the definition of β in terms of a differential approach. As is well known, the conditions of sound propagation in the ocean [19,20] are such that a local interference structure that is resistant to changes in propagation conditions is effectively formed by a small number of constructively interfering modes of the same type. Assuming that the amplitude of the modes is a slower function of their arguments than the phase, one can obtain an expression for the magnitude of [19,20]:

$$\beta_0 = \beta_m(\omega_0) = -\left[\frac{c_{gm}(\omega_0)}{c_{pm}(\omega_0)}\right]^2 \frac{dc_{pm}(\omega_0)}{dc_{gm}(\omega_0)}, \tag{16}$$

where $c_{pm} = \omega/q_m$ and $c_{gm} = d\omega/dq_m$ are the phase and group velocities of the reference m-th mode, in the vicinity of which the modes are in phase. As follows from Eq. (16), the value thus determined depends on the number of reference modes m. It should be noted that Eq. (16) makes it possible, knowing II, to determine the number of m-th mode, which plays a crucial role in the formation of II.

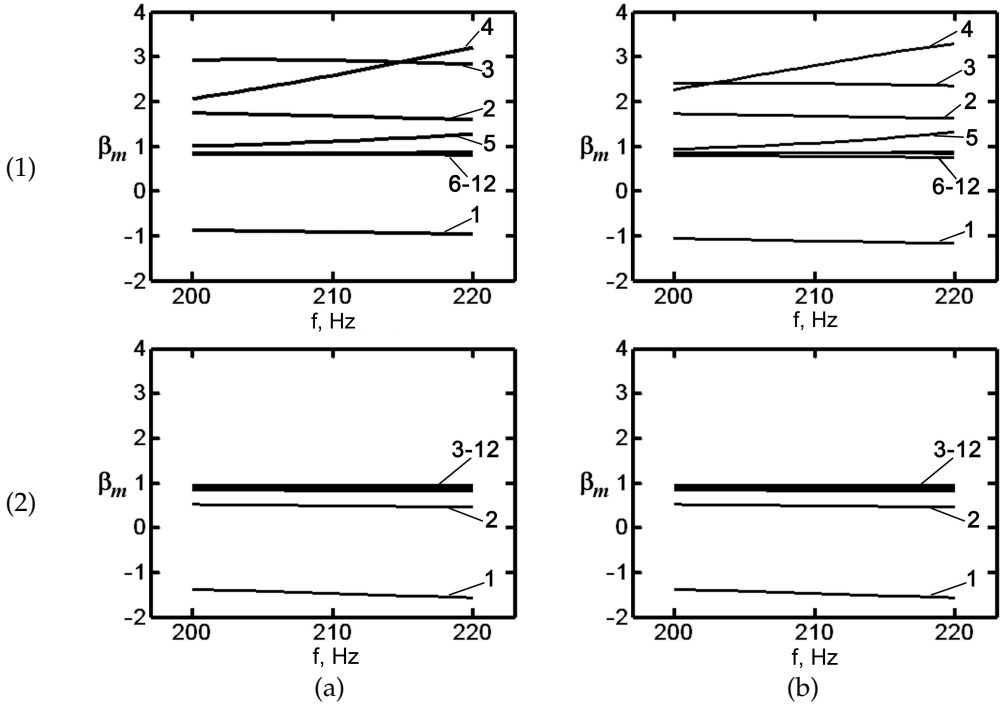

Figure 9. Dependence of value β_m on frequency f at different mode numbers: a) JUSREX (1992); b) SWARM (1995); 1) SW; 2) WW.

As an example, consider a typical water layer stratification observed in the shelf region of the ocean - WW and SW (see Fig. 3). Fig. 10 shows the II dependencies (β_m) on frequency f calculated using Eq. (16) for the stratifications shown in Fig. 3. From Fig. 10 it can be seen that for WW and SW the II value β_m of the first mode is negative and approximately equal, $\beta_1 \approx -1$. For WW, all modes ($m = 3 - 12$) have almost the same value, $\beta_m \approx 1$. The value $\beta_2 \approx 0.7$ slightly deviates from this value 1. In the behavior of β_m for the SW (Fig. 10, 1) there is a clear dependence on the number m. For the group of bottom-surface modes, the behavior of β_m is similar to the behavior in the WW ($\beta_m \approx 1$). These bottom-surface modes are not very sensitive to the expression of the type of sound velocity profile. There is a significant increase in the value of β_m for the bottom modes in SW compared to the corresponding modes in WW ($\beta_2 \approx 1.75$, $\beta_3 \approx 2.5$, $\beta_4 \approx 3.0$). As the frequency increases, the mode number $m = 5$, which lies at the boundary between the bottom and bottom-surface modes, begins to change from one group of modes to another. At the same time, the value β_m starts to increase. At a certain frequency, it assumes a maximum value and then falls. This behavior of the II modal value β_m is related to the transformation of the mode in the SW with increasing frequency. The difference in the behavior of the II modal values β_m should also manifest itself in the different slope of the fringes of the interference structure in the WW and SW. We analyze this difference in the framework of the integral (spectral) approach [25–27,29].

3.2. Integral Approach

Let us consider the sound field intensity distribution $u(r, f)$ (interferogram) Eq. (14) in range-frequency domain (r, f) in the window $r_0 - \Delta r \le r \le r_0 + \Delta r$, $f_0 - \Delta f \le f \le f_0 + \Delta f$:

$$u(r, f) = I(r, f) - \overline{I(r, f)} \tag{17}$$

where $I(r, f)$ - sound field intensity Eq. (14). Here, $\overline{I(r, f)}$ denotes the smoothing over range-frequency window $r_0 - \Delta r \le r \le r_0 + \Delta r$, $f_0 - \Delta f \le f \le f_0 + \Delta f$. We suppose that $u(r, f) = 0$ outside of this window. Let us consider a hologram of the sound field $\tilde{u}(\kappa, \tau)$. Hologram is a result of the two-dimensional Fourier transform (2D-FT) to the

interferogram $u(r,f)$ (Eq. (17)) in the range-frequency domain (r,f). As example, the interferogram $u(r,f)$ and hologram $\tilde{u}(\kappa,\tau)$ (hologram) for SWARM (1995) winter and summer waveguides are presented in Fig. 10. Within framework of the *integral approach* the angular distribution $\Phi(\beta)$ of the hologram $\tilde{u}(\kappa,\tau)$ is analyzed.

$$\Phi(\beta) = \int_0^\infty |\tilde{u}(\rho\cos\vartheta, \rho\sin\vartheta)|^2 \rho\, d\rho, \tag{18}$$

where $\kappa = \rho\sin\vartheta$; $\tau = \rho\cos\vartheta$, (ρ,ϑ) - polar coordinates in (κ,τ) domain ; $\beta = (r_0/\omega_0)\mathrm{tg}\vartheta$.

The maximum $\Phi(\beta)$ falls on the value $\vartheta = \vartheta_0$ corresponding to β_0 - II value. The width $\Delta\beta$ of the function $\Phi(\beta)$ (Fig. 11) determines the error in specifying the position of the maximum of the function $\Phi(\beta)$, i.e., the "blurring" of the direction of observation of the interference fringe. The significance $\Delta\beta$ increases as the number δl of constructively interfering modes decreases. The next width $\Delta\beta$ is evaluated at the level $0.5\Phi(\beta_0)$.

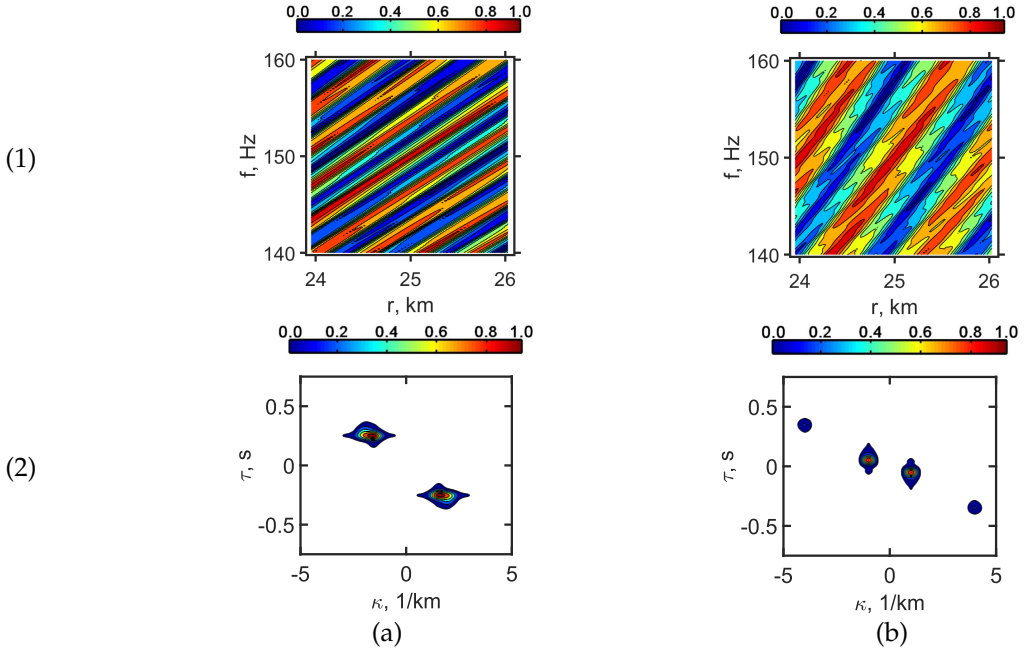

Figure 10. Normalized interferogram (1) and normalized hologram (2) at reference frequency $f = 150$ Hz; a) SWARM (1995) WW; b) SWARM (1995) SW;

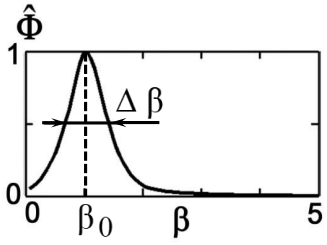

Figure 11. The sound field focal point parameters: width $\Delta\beta$ of the (normalized) function $\Phi(\beta)$.

The width $\Delta\beta$ in the first approximation is equal to:

$$\Delta\beta = \sqrt{\frac{\Phi(\beta)}{d^2\Phi(\beta)/d^2\beta}}\Bigg|_{\beta=\beta_0}. \tag{19}$$

The width value $\Delta\beta$ (Eq. (19)) describes the stability of the interference structure of sound field in the shallow water waveguide. While width value $\Delta\beta$ is insignificant, the interference structure of sound field is stabile. While width value $\Delta\beta$ becomes more significant, the interference structure of sound field losses stability. Thus, the value $\Delta\beta$ can be considered as a measure of the stability of the interference structure of the sound field as a function of distance and frequency variations. The increasing of the width value $\Delta\beta$ is due to two factors. The first of them a decrease of the high modes contribution (modes attenuation) in structure of the sound field. Second one is decrease the length of the interference fringes in which field modes phases are preserved.

The results of the analysis of the interference structure in the framework of the integral approach are shown in Figs. 12 – 14. These figures show the results of computing the distribution of the normalized dependence $\hat{\Phi}(\beta) = \Phi(\beta)/\max[\Phi(\beta)]$. Fig. 12 corresponds to the WW. Fig. 13 - SW. Numerical estimates of the values β_{0j} and $\Delta\beta_j$ corresponding to the dependencies $\Phi(\beta)$ in Fig. 12 and Fig. 13 are given in Table 1 and Table 2, respectively. The dependencies of the quantities $\beta_{0j}(r)$ and $\Delta\beta_j(r)$ on the distance are shown in Fig. 14.

Let us consider the results for the WW. The value β_0 in WW is practically independent of the frequency range and distance. It remains close to $\beta_{0j} \approx 1$ throughout the considered range. The value $\Delta\beta_j$ increases with increasing distance. This effect is explained by the "extinction" of modes with high numbers responsible for the small-scale structure of the distribution $u(r, f)$. This leads to an increase in the contribution of modes with low numbers to the field structure responsible for the large-scale structure of the distribution $u(r, f)$. At short distances ($\sim$ 10 km), the magnitude $\Delta\beta_j$ increases slightly with increasing frequency, which is associated with an increase in the difference between the lower and higher modes (see Fig. 10, 2)). Due to the rapid "depletion" of the mode composition at low frequencies, already at a distance ($\sim$ 50 km) a situation with frequency dependence results $\Delta\beta_j$ turns exactly into the opposite. At distance ($\geq$ 50 km) the width $\Delta\beta_j$ decreases with increasing frequency.

The results corresponding to the SW (Fig. 13) demonstrate the complexity of the interference structure of the sound compared to the WW. In the addition $\Phi(\beta)$, several maxima are observed, resulting from the superposition of interference fringes with different tilt angles. These fringes correspond to different groups of modes.

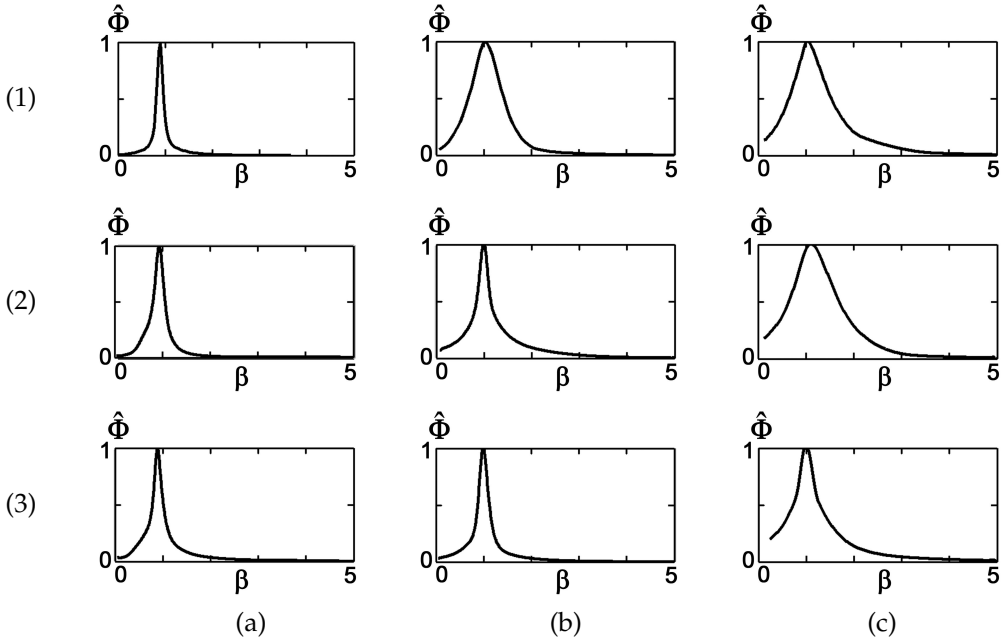

Figure 12. The dependence of the normalized function $\hat{\Phi}$ from parameter β in the neighborhood of distances: a) $r_0 = 10$ km; b) $r_0 = 50$ km; c) $r_0 = 100$ km; 1) $\Delta f_1 = (150 - 170)$ Hz; 2) $\Delta f_2 = (250 - 270)$ Hz; 3) $\Delta f_3 = (350 - 370)$ Hz.

Table 1

	(a)	**(b)**	**(c)**
(1)	$\beta_{01} \approx 0.97$, $\Delta\beta_{01} \approx 0.15$	$\beta_{01} \approx 1.03$, $\Delta\beta_{01} \approx 0.73$	$\beta_{01} \approx 1.01$, $\Delta\beta_{01} \approx 0.91$
(2)	$\beta_{02} \approx 0.99$, $\Delta\beta_{02} \approx 0.25$	$\beta_{02} \approx 0.98$, $\Delta\beta_{02} \approx 0.3$	$\beta_{02} \approx 1.04$, $\Delta\beta_{02} \approx 0.84$
(3)	$\beta_{03} \approx 0.97$, $\Delta\beta_{03} \approx 0.23$	$\beta_{03} \approx 1.01$, $\Delta\beta_{03} \approx 0.24$	$\beta_{03} \approx 1.03$, $\Delta\beta_{03} \approx 0.52$

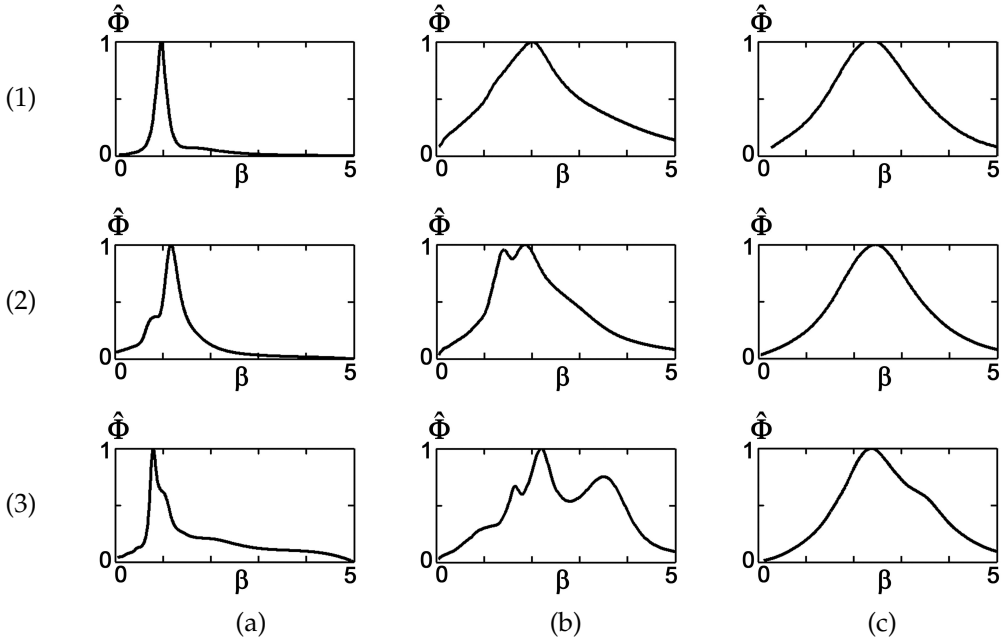

Figure 13. The dependence of the normalized function $\hat{\Phi}$ from parameter β in the neighborhood of distances: a) $r_0 = 10$ km; b) $r_0 = 50$ km; c) $r_0 = 100$ km; 1) $\Delta f_1 = (150 - 170)$ Hz; 2) $\Delta f_2 = (250 - 270)$ Hz; 3) $\Delta f_3 = (350 - 370)$ Hz.

Table 2

	(a)	**(b)**	**(c)**
(1)	$\beta_{01} \approx 0.98$, $\Delta\beta_{01} \approx 0.25$	$\beta_{01} \approx 2.03$, $\Delta\beta_{01} \approx 1.97$	$\beta_{01} \approx 2.50$, $\Delta\beta_{01} \approx 2.02$
(2)	$\beta_{02} \approx 1.18$, $\Delta\beta_{02} \approx 0.4$	$\beta_{02} \approx 1.85$, $\Delta\beta_{02} \approx 1.73$	$\beta_{02} \approx 2.47$, $\Delta\beta_{02} \approx 1.88$
(3)	$\beta_{03} \approx 0.92$, $\Delta\beta_{03} \approx 0.4$	$\beta_{03} \approx 2.15$, $\Delta\beta_{03} \approx 2.43$	$\beta_{03} \approx 2.36$, $\Delta\beta_{03} \approx 2.07$

At short distances from the source ($\sim$ 10 km), bottom-surface modes play a crucial role in the formation of the mode structure of the sound field. As a consequence, at short distances the quantity $\beta_{0j} \approx 1$ over the entire frequency range. As the distance from the source increases, the contribution of the bottom-surface modes decreases significantly and the contribution of the bottom modes increases. As a result, at a distance ($\sim$ 50 km), the AI value $\beta_{0j} \approx 2$ increases. At such distances, the function $\Phi(\beta)$ exhibits, in addition to the main maximum, secondary maxima corresponding to different groups of modes. This is particularly pronounced at higher frequencies (Fig. 13, 3b)). Over long distances ($\sim$ 100 km), the sound field is formed only by bottom modes. This leads to an even stronger increase in the magnitude of II: $\beta_{0j} \approx 2.5$. In this case, the side maxima of the dependencies $\Phi(\beta)$ corresponding to the extinct mode groups disappear. After the distribution $u(r, f)$, they acquire a spotted structure. In this case, the tilt angle of the interference fringes ϑ_0 is larger in the SW than in the WW. The value $\Delta\beta_j$ increases with increasing distance. As in the WW, this is due to the "extinction" of modes with high numbers. In the SW, a certain range of distances is observed where $\Delta\beta_j$ increases sharply. For example, for the frequency range $\Delta f_3 = (350 - 370)$ Hz, at a distance ($\sim$ 50 km) the width reaches $\Delta\beta_3 \approx 2.4$. This is due to the fact that at such distances the bottom modes and the bottom-surface modes make approximately the same contribution to the formation of the sound field. As the distance is further increased, the contribution of the bottom modes becomes dominant. As

a result, the width of the function $\Phi(\beta)$ decreases to the value $\Delta\beta_j \approx 2$. At short distances ($\sim$ 10 km), the magnitude $\Delta\beta_j$ increases more with increasing frequency than in the WW. At longer distances ($\geq$ 50 km), the width $\Delta\beta_j$ decreases with increasing frequency.

The above conclusions are confirmed by the dependence graphs β_{0j} and $\Delta\beta_j$ from the distance shown in Fig. 14 for different frequency ranges.

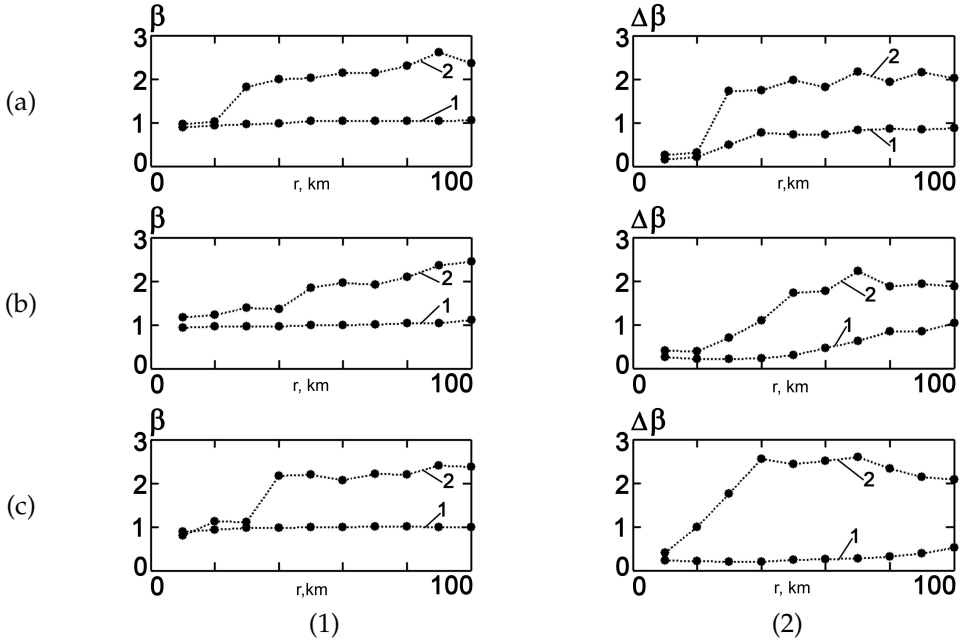

Figure 14. Value dependence β_{0j} and $\Delta\beta_j$ from distance r: a) $\Delta f_1 = (150 - 170)$ Hz; b) $\Delta f_2 = (250 - 270)$ Hz; c) $\Delta f_3 = (350 - 370)$ Hz. Curve 1 - WW. Curve 2 - SW.

4. Sound Field Focalization Control by Frequency Tuning

In this section, the results of the work [30] are further developed and the efficiency of controlling the field focusing by frequency tuning in a regular waveguide with different types of water layer stratification (WW and SW) is investigated.

The sound field is localized by the RTA field at frequency f_0 at RP $Q_0(r_0, z_0)$. When moving to the point $Q(r, z)$ with frequency f_0, the focal spot is destroyed due to the mode dephasing caused by the distance and depth values. The alignment of the mode phases, i.e. the restoration of the sound field focal point is performed by frequency tuning f ($\delta f = f - f_0$ - frequency shift). The frequency tuning allows to shift the undestroyed focal spot to the point $Q(r, z)$ without changing the original distribution of the sound field on the RTA. At the point $Q(r, z)$ the maximum of the sound field $|\Psi(Q)|$ is reached at frequency f. At frequencies deviating from the value f, the sound field value $|\Psi(Q)|$ assumes a lower value.

As an example, we consider a shallow water waveguide (WW and SW) with parameters corresponding to the experiments of JUSREX (1992) [23] and SWARM (1995) [24]. Localization points Q_{ij} (r_i, z_j) with $r_1 = 10$ km, $r_2 = 50$ km, $r_3 = 100$ km; $z_1 = 10$ m, $z_2 = 35$ m, $z_3 = 60$ m. The frequency band $f - \delta f \leq f + \delta f$, where $\delta f = 10$ Hz. The range domain $r - \delta r \leq r + \delta r$, where $\delta r = 2$ km.

The results of modeling the sound field focusing control by frequency tuning are shown in Figs. 15 - 21. Figs. 15 and 16 show the value distribution of the sound field focused on RP $Q_0(r_0, z_0)$ at reference frequency f_0. Fig. 15 corresponds to the reference frequency $f_1 = 150$ Hz, Fig. 16 to the reference frequency $f_2 = 300$ Hz.

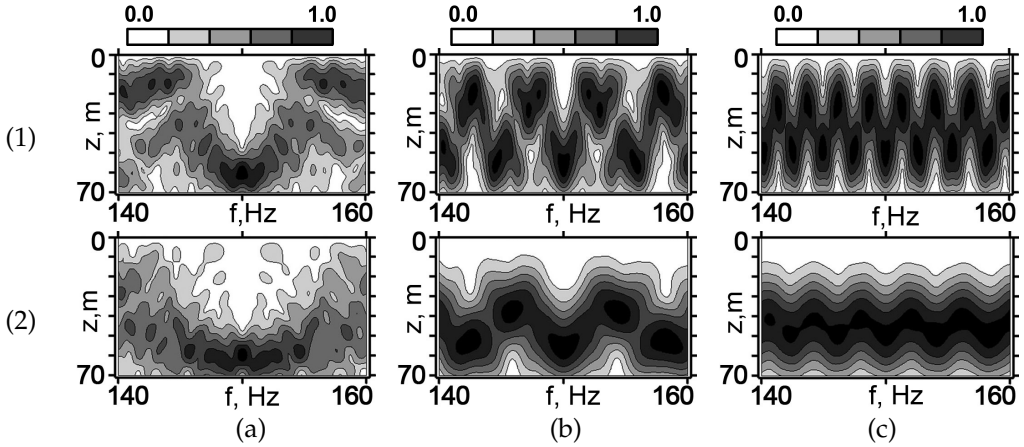

Figure 15. Normalized field distribution $|\Psi(f,z)|$ at frequency $f_1 = 150$ Hz in the vicinity of $Q_{i3}(r_i, z_3 = 60$ m): a) $r_1 = 10$ km, b) $r_2 = 50$ km, c) $r_3 = 100$ km; 1) WW 2) SW

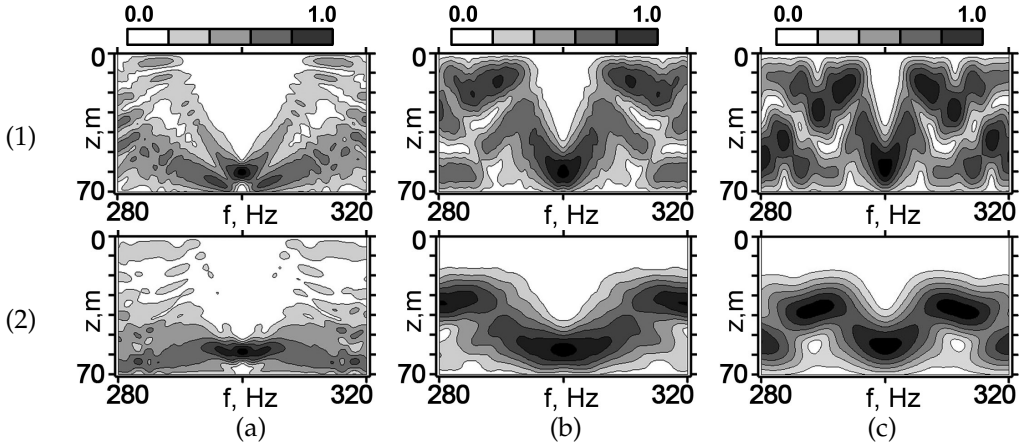

Figure 16. Normalized field distribution $|\Psi(f,z)|$ at frequency $f_2 = 300$ Hz in the vicinity of $Q_{i3}(r_i, z_3 = 60$ m): a) $r_1 = 10$ km, b) $r_2 = 50$ km, c) $r_3 = 100$ km; 1) WW 2) SW.

It can be seen that the frequency band Δf of the focal spot does not behave monotonically with increasing distance r. First Δf increases and then decreases. This can be observed especially in the range of higher frequencies. $f_2 = 300$ Hz. For WW: $\Delta f_1 = 1$ Hz, $\Delta f_2 = 2$ Hz, $\Delta f_3 = 1.5$ Hz. For SW: $\Delta f_1 = 1.37$ Hz, $\Delta f_2 = 5.2$ Hz, $\Delta f_3 = 3.8$ Hz.

Another feature can be seen in the distributions in Figs. 15 and 16. At constant depth, there is a spatial periodicity of the focal points that is most evident in the distributions for distances $r_2 = 50$ km and $r_3 = 100$ km. This effect is a consequence of the property of multimode waveguides to provide spatially periodic (though somewhat poorer) images [31]. Naturally, the magnitudes of the subsequent focal points gradually become blurred, and the amplitude decreases due to the increasing dephasing of the modes. To illustrate the noticed features of the periodicity of focal spots, we consider the parameters of the interference structure of the sound field in the coordinates (r, f). The field distributions in the coordinate system (r, f) at frequency change at depth $z = 60$ m are shown in Fig. 17. The field localization regions are a sequence of interference fringes of different slopes due to the periodic repetition of the focal points. The value of II β and the space period D_l corresponding to Fig. 17 are given in Table 3.

As can be seen from Fig. 17, the angle of the interference fringes θ decreases with increasing range r. The values tgθ for SW exceed the corresponding values for WW by more than twice. The same relation is observed for the II value β related to SW and WW.

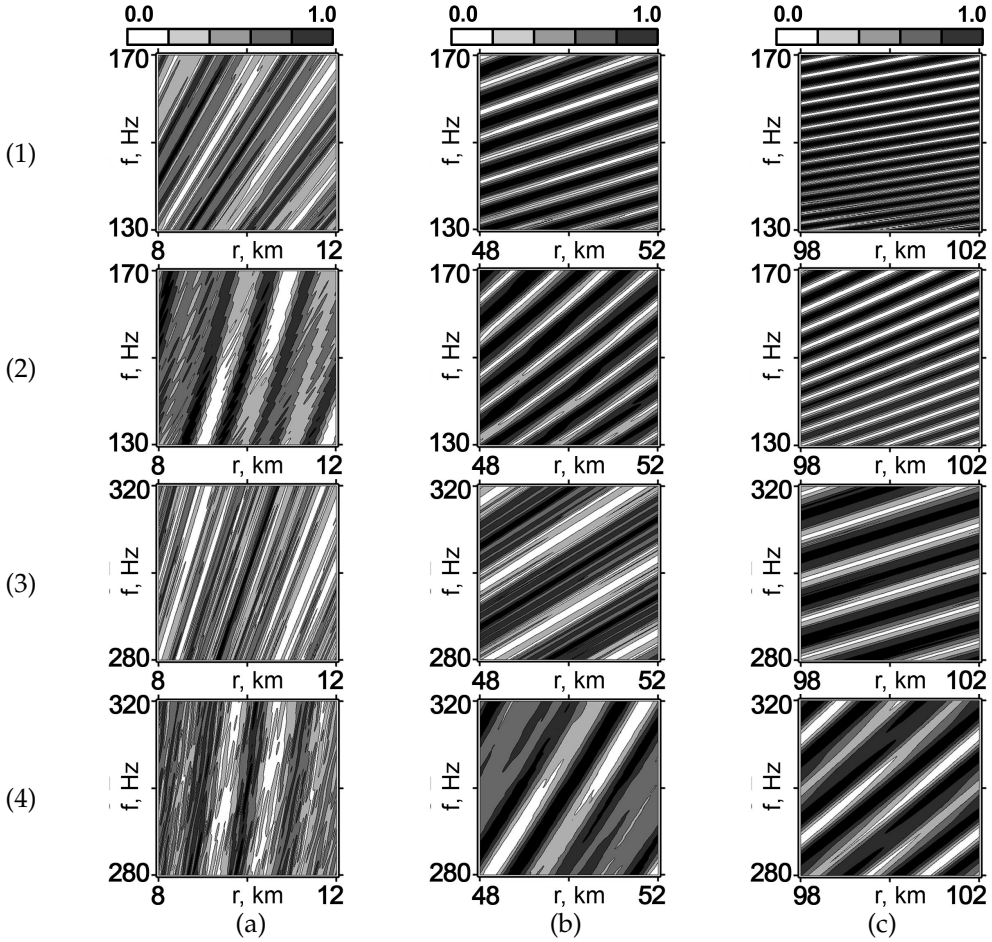

Figure 17. Normalized field distribution $|\Psi(r,f)|$ in the vicinity of $Q_{i3}(r_i, z_3 = 60$ m): a) $r_1 = 10$ km, b) $r_2 = 50$ km, c) $r_3 = 100$ km; 1) $f_1 = 150$ Hz, (WW), 2) $f_1 = 150$ Hz, (SW), 3) $f_2 = 300$ Hz, (WW), 4) $f_2 = 300$ Hz, (SW).

Table 3

	(a)	(b)	(c)
(1)	$\mathrm{tg}\theta \approx 18$ Hz/km, $\beta \approx 1.2$, $D_3 \approx 918$ m	$\mathrm{tg}\theta \approx 3$ Hz/km, $\beta \approx 1.0$, $D_3 \approx 918$ m	$\mathrm{tg}\theta \approx 1.5$ Hz/km, $\beta \approx 1.0$, $D_3 \approx 918$ m
(2)	$\mathrm{tg}\theta \approx 40$ Hz/km, $\beta \approx 2.7$, $D_3 \approx 738$ m	$\mathrm{tg}\theta \approx 8$ Hz/km, $\beta \approx 2.7$, $D_3 \approx 738$ m	$\mathrm{tg}\theta \approx 4$ Hz/km, $\beta \approx 2.7$, $D_3 \approx 738$ m
(3)	$\mathrm{tg}\theta \approx 36$ Hz/km, $\beta \approx 1.2$, $D_3 \approx 965$ m,	$\mathrm{tg}\theta \approx 6$ Hz/km, $\beta \approx 1.0$, $D_3 \approx 965$ m	$\mathrm{tg}\theta \approx 3$ Hz/km, $\beta \approx 1.0$, $D_3 \approx 965$ m
(4)	$\mathrm{tg}\theta \approx 80$ Hz/km, $\beta \approx 2.7$, $D_3 \approx 723$ m,	$\mathrm{tg}\theta \approx 16$ Hz/km, $\beta \approx 2.7$, $D_3 \approx 723$ m	$\mathrm{tg}\theta \approx 8$ Hz/km, $\beta \approx 2.7$, $D_3 \approx 723$ m

Fig. 18 shows the dependence of the tuning frequency $f(r)$ on the distance r as the focal spot moves to an arbitrary point $Q(r, z_0)$.

For given dependencies $f(r)$, radiation frequency tunings are piecewise continuous. The dashed line marks the values of the distance at which the frequency undergoes a jump. The frequency $f(r)$ was calculated as follows. Along the interference fringe (Fig. 17), in the region where the reference point $Q_0(r_0, z_0, f)$ is located, the frequency values f corresponding to the maximum amplitude of the field $|\Psi(r,f)|$ were determined. After passing to the boundaries of the current frequency tuning band f, the transition to the

neighboring band was performed with a frequency jump and along this band the process of calculating the tuning frequency was repeated and so on. The $f(r)$ calculation algorithm was terminated when the limits of the distance change r were reached. Thus, it is possible to control localized fields within a given frequency tuning band by jumping from one band to another. The piecewise continuity of the tuning frequency $f(r)$ is a consequence of the limited area of the focal spot within which the phase relations are preserved.

At the boundary of the region, the phase undergoes a discontinuity that causes a frequency jump necessary to compensate for the change in the phases of the modes as they transit to another region of field focusing. Scanning by focusing occurs on average along straight lines, with slope coefficients tgθ decreasing with increasing distance. This property of the evolution of the slope of the straight lines is related to the invariance of the AI with respect to the distance and the radiation frequency. This continuous region of focal spots corresponds to a dark band in which the reference point and the reference frequency of the radiation are located in the distributions of Fig. 17. There are practically no frequency jumps within this band. The slope coefficients corresponding to these bands are close to the values given above (see Table 3). Thus, scanning with a focal spot in a section of a continuous trajectory is in agreement with the behavior of the II value β. The frequency of focal spot repetition apparently makes it possible to control localized fields at large distances with a narrow frequency band of the source. The limiting distances are, of course, limited by the width of the interval of constructively interfering modes that provide an acceptable quality of focusing.

As an example, we show the structure of the field in coordinates (r, z) near the focal spot, shifted by frequency tuning. On Fig. 19 is shown the distribution of the sound field for the reference point with coordinates Q(50 km, 60 m). The sound field frequency corresponding to Fig. 19 is given in Table 4.

Table 4

	(1)	**(2)**	**(3)**
(a)	$f = 146\ Hz$	$f = 150\ Hz$	$f = 154\ Hz$
(b)	$f = 142\ Hz$	$f = 150\ Hz$	$f = 158\ Hz$
(c)	$f = 292\ Hz$	$f = 300\ Hz$	$f = 308\ Hz$
(d)	$f = 284\ Hz$	$f = 300\ Hz$	$f = 316\ Hz$

For the value $f_1 = 150$ Hz, when the focal spot is shifted by a distance of ± 1 km, the frequency must be tuned to ± 8 Hz in the SW and to ± 4 Hz in the WW. For the value $f = 300$ Hz, the frequency must be tuned to ± 16 Hz in the SW and to ± 8 Hz in the WW. These numerical values of frequency tuning are in good agreement with the parameters of the interference structure of the sound field (Fig. 17) in the vicinity of the focal spot. As can be seen from Fig. 19, scanning with a focal spot by frequency tuning practically does not change the structure of the sound field in coordinates (r, z) in the vicinity of the focal point.

Let us consider the dependence of the focal spot parameters on the scanning distance, taking into account the longitudinal $\Delta r(r)$ and transverse $\Delta z(r)$ focal spot sizes, as well as the relative focusing factor $q(r)$. By the relative focusing factor is meant the value:

$$q(r) = |\Psi(r, z_0, f(r))| / |\Psi(r_0, z_0, f_{1,2})|. \tag{20}$$

Here $|\Psi(r, z_0, f(r))|$ denotes the field amplitude at a point $Q(r, z_0)$, focused by changing the radiation frequency f; $|\Psi(r_0, z_0, f_{1,2})|$ is the amplitude of the focused field at the reference point Q_0 at the reference frequency $f_{1,2}$. The dependence of the focal spot parameters on the distance is shown in Fig. 20, 21. The reference spot depth is 60 m.

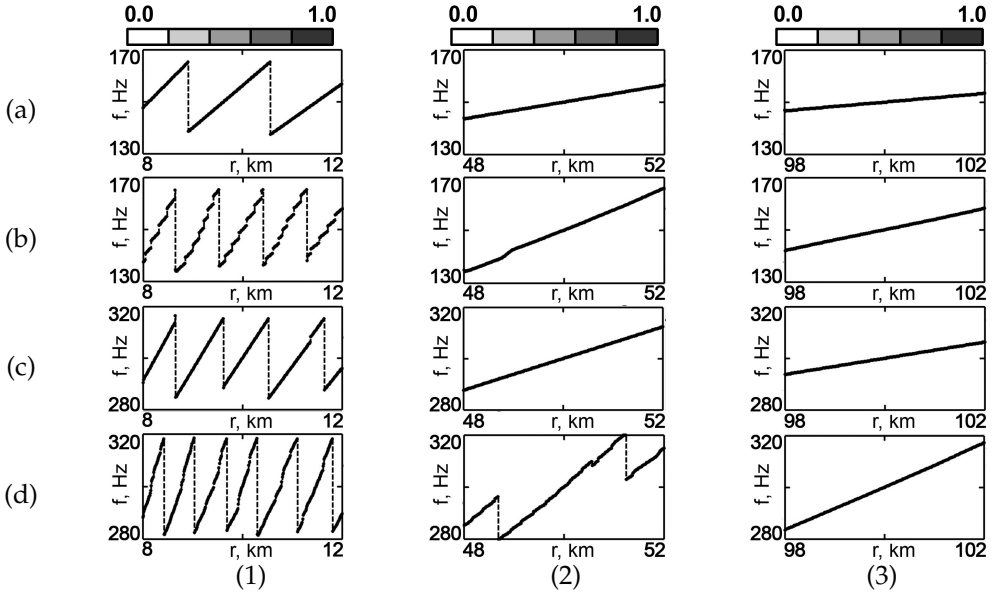

Figure 18. Tuning frequency dependence from range r for controlling of focal spot $Q_{i3}(r_i, z_3 = 60$ m): a) $r_1 = 10$ km, b) $r_2 = 50$ km, c) $r_3 = 100$ km; 1) $f_1 = 150$ Hz, WW, 2) $f_1 = 150$ Hz, SW, 3) $f_2 = 300$ Hz, WW, 4) $f_2 = 300$ Hz, SW.

As can be seen, the parameters of the focal spot are smoother (more stable) during frequency tuning in the WW. This can be explained by the fact that the interference structure in the SW consists of modes with significantly different spatial scales. The instability of the focal spot parameters is more pronounced at high frequencies and decreases with decreasing frequency. Moreover, the instability of the focal spot parameters decreases with increasing distance from the reference point as the fraction of bottom-surface modes decreases. Regions with strong changes in magnitude q correspond to neighborhoods of tuning frequency jumps f. It should also be noted that the value q increases as the focal spot $Q \neq Q_0$ is shifted forward to RTA. There are two processes that influence the value of q. One of processes is sound modes dephasing due to focal spot shift. The modes dephasing leads to a decreasing of focal spot value q for both cases: shift forward RTA and shift from RTA. Second of processes is sound modes attenuation. The modes attenuation leads to a increasing of focal spot value for case of shift to RTA and to decreasing of focal spot value in case of shift from RTA. The process cased by modes attenuation is stronger than process cased by modes dephasing for short range ($r = 10km$). As result focal spot shift to RTA leads to increasing of focal spot value q. In contrast to short range ($r = 10km$), at long range ($r = 100km$) the focal spot value $q(r)$ is decreases for both cases: shift forward RTA and shift from RTA. This is due to a decrease high modes contribution (modes attenuation) in structure of the sound field with range increasing.

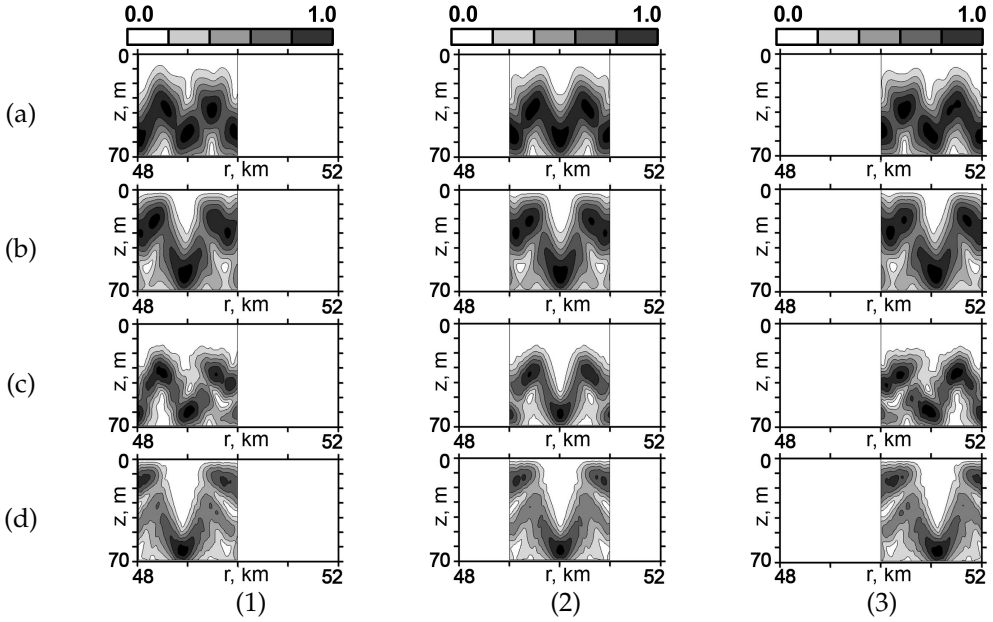

Figure 19. Focal spot scanning $Q_{23}(r_2 = 50$ km, $z_3 = 60$ m): a) $f_1 = 150$ Hz, WW, b) $f_1 = 150$ Hz, SW, c) $f_2 = 300$ Hz, WW, d) $f_2 = 300$ Hz, SW; 1) $Q(r = 49$ km, $z = 60$ m), 2) $Q(r = 50$ km, $z = 60$ m), 3) $Q(r = 51$ km, $z = 60$ m).

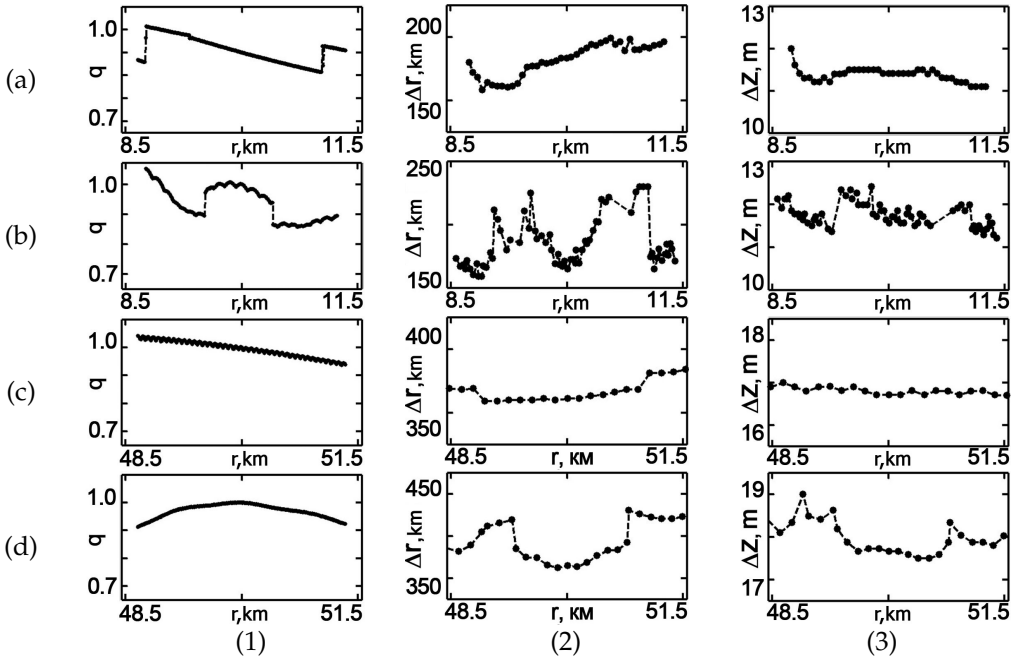

Figure 20. The dependence of the focal spot parameters from r for $f_1 = 150$ Hz: 1) $q(r)$, 2) $\Delta r(r)$, 3) $\Delta z(r)$; a) $r_1 = 10$ km, WW, b) $r_1 = 10$ km, SW, c) $r_2 = 50$ km, WW, d) $r_2 = 50$ km, SW.

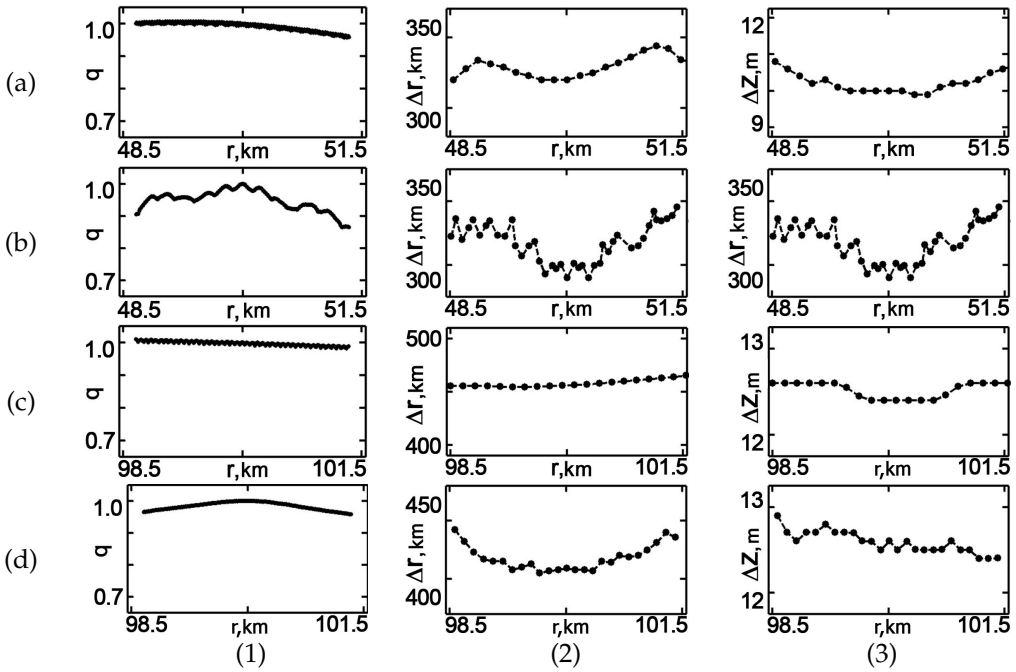

Figure 21. The dependence of the focal spot parameters from distance r for $f_2 = 300$ Hz: 1) $q(r)$, 2) $\Delta r(r)$, 3) $\Delta z(r)$; a) $r_2 = 50$ km, WW, b) $r_2 = 50$ km, SW, c) $r_3 = 100$ km, WW, d) $r_3 = 100$ km, SW.

5. Conclusions

The possibility of controlling localized fields in multimode shallow water waveguides based on the principle of interference invariance have been studied. Within framework of the numerical experiments in a wide frequency range of 100 - 350 Hz and range intervals of 10 -100 km, the possibilities of focusing the sound field by WFR and controlling of the focusing of the focal spot by frequency tuning in shallow water waveguide have been analysed. The spatial focusing by WFR consists of recording the sound field from a distant probe source by RTA, reversing of the recording signals by phase conjugation and propagating the reversed signal back in shallow water waveguide. In result the sound field is spatially focused at the probe source location. The focal spot scanning is carried out by frequency tunning with a fixed distribution of the sound field at RTA aperture. A comparative analysis of the features of focusing and focal spot control for summer and winter stratification of the water layer is carried out. It is shown that the parameters of the focal spot during frequency tuning are more stable in the winter waveguide. It is shown that the parameters of the focal spot during frequency tuning are more stable in the winter waveguide. It is demonstrated that the sound frequency tuning has a piecewise continuous character and is carried out on a domain of one continuous track and jump-passing on other track in accordance with the waveguide interference fringes in range-frequency domain.

Of course, these conclusions are not related to the special choice of this waveguide model. For different shallow water waveguide model, the qualitative situation of the focal spot controlling by frequency tunning is preserved. However, quantitative estimates of the focal spot parameters are different. It is important for offered method focal spot controlling by frequency tunning that the interference invariant in shallow water waveguide remains applicable. In this case the regular interferential pattern of sound field is formed. It is mean that amplitudes of the sound field modes are a slower function of range in comparison to the modes phase. This condition, which underlies the formation of an interference invariant [19] imposes restrictions both on the nature of the shallow water waveguide and on the range of focal spot scanning.

Author Contributions: Supervision and project administration, M.E.; conceptualization and methodology, V.K. and S.P.; software, S.T. and P.R.; validation, M.E. and V.K.; formal analysis, M.E. and S.P.;

writing – original draft preparation, M.E. and S.P.; writing – review and editing, M.E. and S.P.; All authors have read and agreed to the published version of the manuscript.

Funding:
This work was supported in part by the Ministry of Education and Science of the Russian Federation through Project No. FZGU-2023-0007
S.A. Tkachenko's work was supported by the grant of the President of the Russian Federation, (project no. MK-4846.2022.4).

References

1. Weston, D. "Sound Focusing and Beaming in the Interference Field Due to Several Shallow-Water Modes,", J. Acoust. Soc. Amer. **44**(6), 1706-1712 (1968).
2. Dargeoeko, M. M., Kravtsov, Yu. A., Petnikov, V. G., Petrosyan, A. S., Samoilenko, Yu. I., and Slavinskii, M. M. (**1984**). "Unique features of radiation field focusing in multimode waveguide channels," Radiophys. Quant. Electr. **27**(6), 516–522.
3. Danilov, V. Ya., Kravtsov, Yu. A., and Nakonechny, A. G. (**1991**). "Mathematical aspects of hydroacoustic field control," in *Formation of Acoustic Fields in Oceanic Waveguides*, (Inst. Prikl. Fiz., Akad. Nauk SSSR), pp. 32–54.
4. Jackson, D. and Dowling, D. "Phase conjugation in underwater acoustics,", J. Acoust. Soc. Amer. **89**, 171-181 (1991).
5. Dowling, D. and Jackson, D. "Narrow-band performance of phase-conjugate arrays in dynamic random media,", J. Acoust. Soc. Amer. **91**, 3257-3277 (1992).
6. Tao, H. and Krolik, J. "Waveguide invariant focusing for broadband beamforming in an oceanic waveguide,", J. Acoust. Soc. Amer. **123**, 1338 (2008).
7. Prada, C., Rosny, J., Clorennec, D., Minonzio, J., Aubry, A., Minonzio, J., Fink, M., Berniere, L., Billand, P., Hibral, S., and Folegot, T. "Experimental detection and focusing in shallow water by decomposition of the time reversal operator.,", J. Acoust. Soc. Amer. **122**(2), 761 (2005).
8. Walker, S., Kuperman, W., and Roux, Ph. "Focal depth shifting of a time reversal mirror in a range-independent waveguide,", J. Acoust. Soc. Amer. **118**, 1341 (2005).
9. Walker, S., Kuperman, W., and Roux, Ph. "Active waveguide Green's function estimation with application to time-reversal focusing without a probe source in a range-independent waveguide,", J. Acoust. Soc. Amer. **120**, 2755 (2006).
10. Kuperman, W., Hodgkiss, W., and Song, H. (**1998**). "A time-reversal mirror with variable range focusing," J. Acoust. Soc. Amer. **103**(6), 3234-3240.
11. Kuperman, W., Hodgkiss, W., and Song, H. (**1998**). "Phase conjugation in the ocean: Experimental demonstration of an acoustic time-reversal mirror," J. Acoust. Soc. Amer. **103**(1), 25-40.
12. Fink, M. "Time-reversal mirror,", J. Phys. D **26**, 1330-1350 (1993).
13. Fink, M., Cassereau, D., Derode, A., Prada, C., and Roux, P. (**2000**). "Time-reversed acoustics," Rep. Prog. Phys. **63**, 1933–1995.
14. Pereselkov, S. and Lun'kov, A. "Specific features of surface reverberation in shallow water with focused sound field,", J. Acoust. Soc. Amer. **123**, 3596 (2008).
15. Pereselkov, S. and Petnikov, V. "Sound focusing and scanning in shallow water with background internal wave field,", J. Acoust. Soc. Amer. **123**, 3595 (2008).
16. Talanov, V. (**1985**). "On the synthesis of antennas in a multimode waveguide," Izv. Vyssh. Uchebn. Zaved., Radiofiz. **28**(7), 872-880.
17. Gorodetskaya, E. Yu. Malekhanov, A. I., and Talanov, V. I. (**1994**). "Adaptive control of acoustic fields in oceanic waveguides," in *Formation of Acoustic Fields in Oceanic Waveguides: Reconstruction of Inhomogeneities*, (Inst. Prikl. Fiz., Ross. Akad. Nauk), pp. 9–43.
18. Weston, D. and Stevens, K. "Interference of wide-band sound in shallow water,", J. Sound Vibr. **21**(1), 57–64 (1972).
19. Chuprov, S., "Interference structure of a sound field in a layered ocean,", Ocean Acoustics, Current State 71–91 (1982).
20. Grachev, G. and Wood, J., "Theory of acoustic field invariants in layered waveguides,", Acoust. Phys. **39**(1), 33–35 (1993).
21. Orlov, E. F., and Sharonov, G. A. (**1998**). "Interference of sound waves in the ocean,", (Dal'nauka).
22. Kuperman, W. A. and D'Spain, G. L., "Ocean acoustic interference phenomena and signal processing,", Ocean Acoust. Interfer. Phen. Signal Process. **621** (2002).
23. Gasparovic, R. F. and Etkin, V. S., "An overview of the Joint US/Russia Internal Wave Remote Sensing Experiment,", Proceedings of IGARSS '94 - 1994 IEEE International Geoscience and Remote Sensing Symposium, 741–743 (1994).
24. Apel, J. R., Badiey, M., Chiu, C.-S., Finette, S., Headrick, R., Kemp, J., Lynch, J.F., Newhall, A., Orr, M.H., Pasewark, B.H., Tielbuerger, D., Turgut, A., Von Der Heydt, K., and Wolf, S., "An overview of the 1995 SWARM shallow-water internal wave acoustic scattering experiment,", IEEE J. Ocean. Engrg., 465–500 (1997).
25. Rouseff, D., "Effect of shallow water internal waves on ocean acoustic striation patterns,", Waves in Random Media **11**, 377–393 (2001).
26. Rouseff, D., and Spindel, R. C. (**2002**). "Modeling the waveguide invariant as a distribution," AIP Conf. Proc. **621**, 137–150.
27. Baggeroer, A. B. (**2002**). "Estimation of the distribution of the interference invariant with seismic streamers," AIP Conf. Proc. **621**, 151–170.
28. Pereselkov, S. Kuz'kin, V. "Interferometric processing of hydroacoustic signals for the purpose of source localization,", J. Acoust. Soc. Amer. **151**, 666-676 (2022).

29. Ehrhardt, M., Pereselkov, S., Kuz'kin, V., Kaznacheev, I., and Rybyanets, P. (**2023**). "Experimental observation and theoretical analysis of the low-frequency source interferogram and hologram in shallow water," J. Sound Vibr. **544**(3), 117388
30. Grigor'ev, V., Kuz'kin, V., (**2005**). "Field focusing control in multimode plane-layered waveguides," Acoust. Phys. **51**, 292–299
31. Grigor'eva, E., Semenov, A., (**1978**). "Waveguide image transmission in coherent light (review)," Sov. J. Quant. Electron. **8**, 1063